

Particle settling in a fluctuating multicomponent fluid under confinement

Xiao Xue,^{1,2,*} Luca Biferale,^{2,†} Mauro Sbragaglia,^{2,‡} and Federico Toschi^{3,4,§}

¹*Department of Physics and J.M. Burgerscentrum,
Eindhoven University of Technology, 5600 MB Eindhoven, the Netherlands.*

²*Department of Physics & INFN, University of Rome “Tor Vergata”,
Via della Ricerca Scientifica 1, 00133, Rome, Italy.*

³*Departments of Physics and of Mathematics and Computer Science and J.M. Burgerscentrum,
Eindhoven University of Technology, 5600 MB Eindhoven, the Netherlands.*

⁴*Istituto per le Applicazioni del Calcolo CNR, Via dei Taurini 19, 00185 Rome, Italy.*

We study the motion of a spherical particle driven by a constant volume force in a confined channel with a fixed square cross-section. The channel is filled with a mixture of two liquids under the effect of thermal fluctuations. We use the lattice Boltzmann method to simulate a fluctuating multicomponent fluid in the mixed-phase, and particle-fluid interactions are tuned to reproduce different wetting properties at the particle surface. The numerical set-up is first validated in the absence of thermal fluctuations; to this aim, we quantitatively compute the drift velocity at changing the particle radius and compare it with previous experimental and numerical data. In the presence of thermal fluctuations, we study the fluctuations in the particle’s velocity at changing thermal energy, applied force, particle size, and particle wettability. The importance of fluctuations with respect to the mean drift velocity is quantitatively assessed, especially in comparison to unconfined situations. Results show that confinement strongly enhances the importance of velocity fluctuations, which can be one order of magnitude larger than what expected in unconfined domains. The observed findings underscore the versatility of the lattice Boltzmann simulations in concrete applications involving the motion of colloidal particles in a highly confined environment in the presence of thermal fluctuations.

PACS numbers: 47.61.-k, 05.40.-a, 05.40.Jc, 05.10.Gg

Keywords: Fluctuating Lattice Boltzmann Models, Binary Mixtures, Brownian Motion

I. INTRODUCTION

Complex flow phenomena involving dispersions of particles moving in viscous fluids are of interest for their theoretical relevance in the framework of non-equilibrium statistical mechanics [1, 2]. Such phenomena are also relevant in a variety of applications, ranging from large [3] to small scales [4]. The corresponding theoretical description at the large scales hinges on the deterministic Navier-Stokes equations [5, 6], suitably coupled to the surface of the particles via hydrodynamic boundary conditions; these, in turn, account for the affinity of the particle towards the fluid and result in macroscopic properties, such as slip, wettability, etc. The deterministic dynamics of the Navier-Stokes equations is however fairly inadequate for the description at smaller scales, where the assumptions of negligible fluctuations cease to be valid [7, 8]. In these conditions, mesoscale methods represent methods of choice [9]. By definition, mesoscale modeling is constructed at scales which are intermediate between the large scales and the small scales; hence, a suitable coarse-graining allows to recover the hydrodynamical description based on the Navier-Stokes equations. Additionally, one can enrich the modeling with nanoscale features like thermal fluctuations [7, 8]. Among all mesoscale methods, we are interested in the lattice Boltzmann models (LBM). Over the last decades, LBM have been successfully used to model complex hydrodynamic phenomena at large scales, such as particle suspensions [4, 10, 11], non-ideal fluids with phase transition and/or phase segregation [12–17], polymer flows [18–20], active matter [21] just to cite some prominent examples. Especially in the last decade, there has been a boost to push the applicability of LBM simulations towards nano-scales via the inclusion of thermal fluctuations [22–27], designing the so-called *fluctuating lattice Boltzmann* methodology (FLBM). This methodology has been recently applied to the study of multicomponent fluids in the presence of thermal fluctuations [28, 29] and also to study the effects of thermally excited capillary waves on the break-up properties of a thin liquid ligament [30]. In this paper, we propose a novel application of the FLBM. Specifically, we quantitatively characterize the motion of a spherical colloidal particle driven by a constant volume

*Electronic address: X.Xue@tue.nl

†Electronic address: biferale@roma2.infn.it

‡Electronic address: sbragaglia@roma2.infn.it

§Electronic address: F.Toschi@tue.nl

force in a confined nanofluidic channel. The channel is filled with a fluctuating multicomponent mixture of two fluids. The FLBM is particularly versatile in allowing the characterization of the particle's velocity fluctuations at changing the various free parameters in the problem, i.e. the particle radius, the thermal energy, the driving force, and the particle wettability. From one side, we will show that the results of the simulations quantitatively agree with the prediction of a Langevin equation with Gaussian noise and effective friction that accounts for the effects of confinement. From the other side, we will compare the particle's velocity fluctuations to its mean drift velocity, highlighting the difference between unconfined and confined situations. The paper is organized as follows. In Section II, we summarize the essential methodological aspects of the FLBM for multicomponent fluids and the coupling between particles and the multicomponent fluid. In Section III we will present the set-up for the numerical simulations and we will present validation studies in the absence of thermal fluctuations, by comparing the drift velocity with previous experimental and numerical data. Results in the presence of thermal fluctuations will be presented in Section IV. Conclusions will follow in Section V.

II. METHODOLOGY

To model the bulk fluid, we consider LBM that allow for the simulations of multicomponent mixture of two components in the presence of thermal fluctuations [28]. We additionally introduce finite-size particles via a suitable coupling between the particle and the multicomponent fluid [31–33]. The essential technical details of the LBM used here are briefly summarized, the interested reader can refer to the reference works [28, 31–33] for more extensive technical coverage.

The multicomponent LBM considers the evolution equation of probability distribution functions, $f_{li}(\mathbf{x}, t)$, representing the probability density to find a particle of fluid component $l = A, B$ with kinetic velocity \mathbf{c}_i in the space-time location (\mathbf{x}, t) . Lattice velocities are discretized ($i = 0, 1, \dots, Q - 1$) and we employ the D3Q19 model, with $Q = 19$ velocity directions. The density of each component and the mixture velocity can be obtained via a proper coarse-graining in the kinetic velocity

$$\rho_l(\mathbf{x}, t) = \sum_{i=0}^{Q-1} f_{li}(\mathbf{x}, t), \quad \rho_{\text{tot}}(\mathbf{x}, t)\mathbf{v}(\mathbf{x}, t) = \sum_{i=0}^{Q-1} \sum_{l=A,B} f_{li}(\mathbf{x}, t)\mathbf{c}_i \quad (1)$$

being $\rho_{\text{tot}}(\mathbf{x}, t) = \sum_{l=A,B} \rho_l(\mathbf{x}, t)$ the total density. The evolution equation for the distribution functions over a unitary time step is given by

$$f_{li}(\mathbf{x} + \mathbf{c}_i, t + 1) - f_{li}(\mathbf{x}, t) = \mathcal{L} \left[f_{li}(\mathbf{x}, t) - f_{li}^{(eq)}(\mathbf{x}, t) \right] + S_{li}^{(F)}(\mathbf{x}, t) + \xi_{li}(\mathbf{x}, t) \quad l = A, B. \quad (2)$$

The collision operator \mathcal{L} is designed in such a way that it expresses the relaxation of the whole system towards a local Maxwellian distribution function $f_{li}^{(eq)}(\mathbf{x}, t)$ [9, 34]. Technically, we make use of the MRT (multiple relaxation time) scheme [25, 35, 36]: the distribution functions are decomposed in modes (density, momentum, stress, etc) and the action of \mathcal{L} consists in relaxing the different modes with different relaxation times [35]. The relaxation time of the momentum modes will determine the species diffusivity [25], whereas the relaxation time of the stress modes will determine the fluid viscosity [25, 35]. The term $S_{li}^{(F)}(\mathbf{x}, t)$ is a deterministic source term, accounting for the external volume forces and the interactions between the two components. For the modelling of non-ideal interactions, we adopt the Shan-Chen formulation for multicomponent mixtures [37–41], where the force experienced by the fluid component l due to the surrounding fluid component l' can be written as

$$F_l(\mathbf{x}, t) = -\mathcal{G}\rho_l(\mathbf{x}, t) \sum_{l' \neq l} \sum_{i=0}^{Q-1} \omega_i \rho_{l'}(\mathbf{x} + \mathbf{c}_i, t)\mathbf{c}_i \quad (3)$$

where \mathcal{G} is a strength coefficient and ω_i a suitable weight needed to impose the isotropy in the interactions [37, 38, 40]. In all the simulations performed, we consider a non-ideal mixture with $\mathcal{G} = 1.5$ (lattice Boltzmann units, lbu) and we simulate a bulk fluid with a majority of component A and fluid densities $\rho_A = 2.21$ lbu (majority component) and $\rho_B = 0.09$ lbu (minority component). The term $\xi_{li}(\mathbf{x}, t)$ is a stochastic force, which adds to the deterministic evolution a stochastic term. The stochastic terms are chosen in such a way that the conserved mass densities do not receive any stochastic force, while non-conserved modes receive a stochastic force in compliance with the fluctuation-dissipation relation [28]. Eq. (2) implies evolution equations for macroscopic density and velocity. If we apply a Chapman-Enskog procedure [25, 36], the macroscopic equations of a binary mixture in the presence of thermal fluctuations [8]

are recovered for the fluid densities and the hydrodynamical velocity $\mathbf{v}^{(H)} = \mathbf{v} + (\mathbf{F}_A + \mathbf{F}_B)/2\rho_{\text{tot}}$ (superscript T means transposition)

$$\partial_t \rho_{\text{tot}} + \nabla \cdot (\rho_{\text{tot}} \mathbf{v}^{(H)}) = 0 \quad (4)$$

$$\partial_t (\rho_{\text{tot}} \mathbf{v}^{(H)}) + \nabla (\rho_{\text{tot}} \mathbf{v}^{(H)} \mathbf{v}^{(H)}) = -\nabla P_b + \nabla \cdot [\eta (\nabla \mathbf{v}^{(H)} + (\nabla \mathbf{v}^{(H)})^T) + \boldsymbol{\Sigma}_{\text{tens}}] + \rho_{\text{tot}} \mathbf{g} \quad (5)$$

$$\partial_t \rho_A + \nabla \cdot (\rho_A \mathbf{v}^{(H)}) = \nabla \cdot [D \nabla \mu + \boldsymbol{\Psi}_{\text{vec}}] \quad (6)$$

where the bulk pressure P_b and the chemical potential μ assume the form $P_b = \frac{1}{3} \rho_{\text{tot}} + \frac{c}{3} \rho_A \rho_B$ and $\mu = \frac{1}{3} \log \rho_A - \frac{1}{3} \log \rho_B + \frac{1}{3} \mathcal{G}(\rho_A - \rho_B)$ [28], \mathbf{g} is external volume force acting on the fluid. The transport coefficients D and η are related to the relaxation times of the fluid. These will be fixed to $D = 1/6$ lbu and $\eta = 0.383$ lbu in all the simulations performed. The capital Greek symbols identify the stochastic stress ($\boldsymbol{\Sigma}_{\text{tens}}$) and the stochastic diffusion ($\boldsymbol{\Psi}_{\text{vec}}$) contributions to the equations of hydrodynamics

$$\boldsymbol{\Sigma}_{\text{tens}} = \sqrt{\eta k_B T} (\mathbf{W}_{\text{tens}} + \mathbf{W}_{\text{tens}}^T) \quad \boldsymbol{\Psi}_{\text{vec}} = \sqrt{2D k_B T} \mathbf{W}_{\text{vec}} \quad (7)$$

where $k_B T$ is the thermal energy, while \mathbf{W}_{tens} and \mathbf{W}_{vec} are a Gaussian tensor and a Gaussian vector with independent and uncorrelated components and variance equal to unity. For the LBM modelling of the particle, we follow References [31–33]. The particle is modelled on the lattice, by declaring the fluid nodes belonging to the particle (“particle nodes”), as sketched in Fig. 1. The dynamical evolution of the particle is solved with the leap-frog algorithm [42]. The bounce back boundary condition is implemented at the interface between the particle and the fluid [31]. During the bounce back procedure, the particle exchanges the momentum with the surrounding fluid. Due to the particle movement in the fluid, there will be the creation of new particle nodes which originally were fluid nodes (cover-nodes behavior). Analogously, the movement of the particle can delete the particle nodes and create new fluid nodes (uncover-nodes behavior). In order to impose the total mass conservation, we implement the mass correction algorithm described in [33]. Also, we introduce a virtual fluid layer [33] at the interface between the particle and the fluid to be able to tune the particle’s wettability. In such a layer, the fluid densities are set equal to the average densities of the neighbouring fluid nodes, plus a correction $\Delta \rho$ that is instrumental to model the affinity of the particle towards the two components. The wettability properties described in the following (i.e. hydrophobic, neutral, hydrophilic) refer to the affinity of the particle towards the majority component in the bulk phase.

III. NUMERICAL SET-UP AND VALIDATION

The set-up for the numerical simulations is sketched in Fig. 1. A particle with diameter d is placed in a long channel with square cross section $L \times L$. The particle is initially placed with its center of mass lying in the center of the square cross-section and is driven by a volume force, \mathbf{g} , acting in the z direction. The resulting force on the particle is

$$\mathbf{F}_p = \frac{4}{3} \pi \left(\frac{d}{2} \right)^3 (\rho_p - \rho_{\text{tot}}) \mathbf{g} \quad (8)$$

where ρ_p is the particle density which is set to $\rho_p = 2\rho_{\text{tot}}$. The channel is resolved with $L \times L \times L_z = 60 \times 60 \times 900$ lbu. The channel is closed with walls in all directions; this choice is instrumental to fully appreciate the effects of confinement. A neutral wettability boundary condition is chosen for all the bounding walls, while three different wettabilities are considered at the interface between the particle and the fluid: these correspond to wetting angles $\theta = 120.5$, $\theta = 90^\circ$, $\theta = 55.0$ and will be denoted hereafter as “hydrophobic”, “neutral” and “hydrophilic”. The square cross section is kept fixed in all numerical simulations, while different particle’s diameters are considered. Different values of the thermal energy and driving force are also simulated. The simulations parameters are chosen in the following ranges: $d/L \in [0.133 : 0.67]$, $k_B T \in [1 \cdot 10^{-5} : 0.45 \cdot 10^{-3}]$ lbu, $\mathbf{g} \in [5 \cdot 10^{-7} : 5 \cdot 10^{-5}]$ lbu.

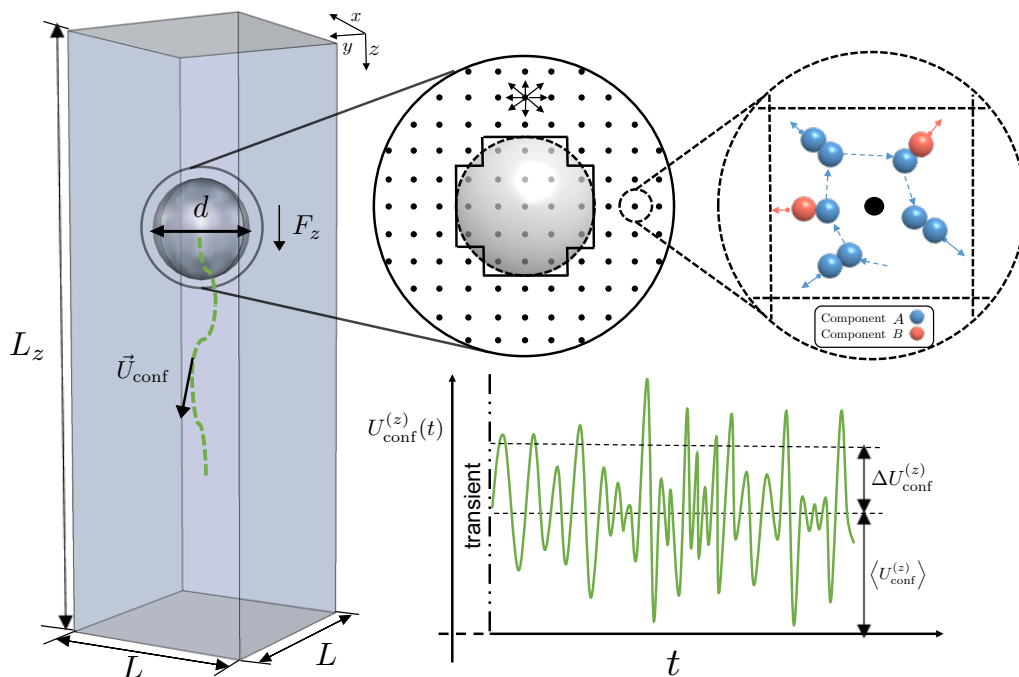


FIG. 1: Sketch of the setup for the particle settling numerical simulations. The computational box is a rectangular parallelepiped of height L_z and square base $L \times L$. The solvent fluid is a fluctuating mixture of two non-ideal components, A and B , with majority of the component A in the bulk phase. The whole system is under the effect of the volume force, g , acting in the z direction. The mixture and the particle are simulated using lattice Boltzmann models (LBM) on a regular three dimensional lattice (cfr. Section II). The LBM implementation is further equipped with thermal fluctuations (fluctuating LBM, FLBM [28]) to mimic the effect of noise at the small scales. The particle's velocity is tracked as a function of time and we quantify its statistical properties (average $\langle U_{\text{conf}}^{(z)} \rangle$) and fluctuations $\Delta U_{\text{conf}}^{(z)}$ in the statistically steady state.

We have first validated the numerical set-up without thermal fluctuations. To this aim, we measured the steady drift velocity of the particle at changing the particle diameter. The steady drift velocity in the confined (conf) channel will be proportional to the driving force and inversely proportional to the friction γ_{conf}

$$U_{\text{conf}}^{(z)} = \frac{F_p}{\gamma_{\text{conf}}}. \quad (9)$$

In unconfined (unconf) domains one would expect the Stokes-law for the friction $\gamma_{\text{unconf}} = 3\pi\eta d$. However, it is known from the literature that confinement enhances friction and reduces the drift velocity in comparison to the unconfined cases [43–47]. We therefore focused the attention on the ratio c_m as a function of d/L . c_m is defined as the ratio between the particle's drift velocity under confinement and the Stokes' prediction for an unconfined particle driven by the same volume force

$$c_m(d/L) = \frac{U_{\text{conf}}^{(z)}}{U_{\text{unconf}}^{(z)}}. \quad (10)$$

To keep the notation simple, $c_m(d/L)$ will be replaced by c_m in the rest of the article. Results are in good agreement with the experimental observations. Discrepancies which may be observed with coarser grids (results from [32]) become essentially negligible with our finer grids. We also observe that there is almost no dependency on the wettability condition.

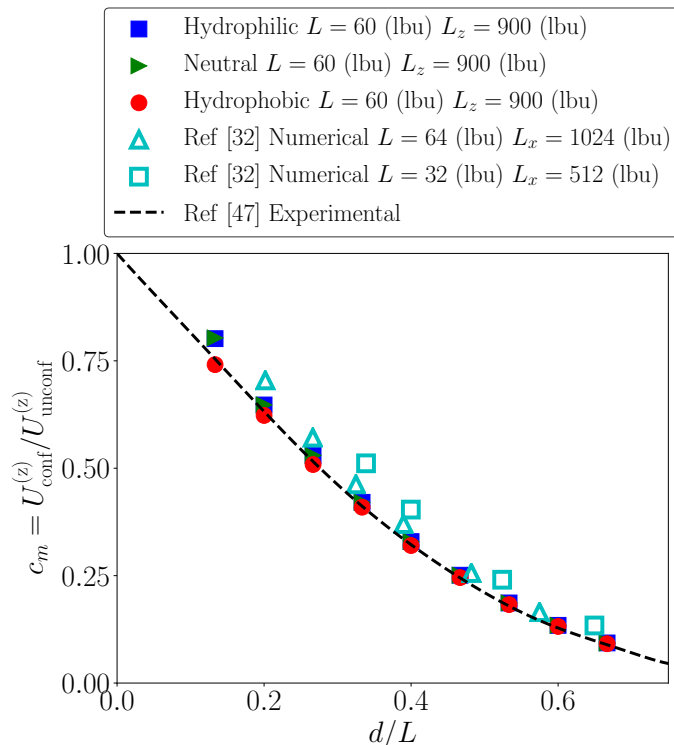


FIG. 2: We report the ratio, c_m , between the particle’s drift velocity under confinement and the Stokes’ prediction for an unconfined particle driven by the same volume force (cfr. Eq. (10)). The ratio c_m is considered as a function of the degree of confinement d/L (cfr. Fig. 1) and for different wettability boundary conditions at the particle’s surface: hydrophilic (blue squares), neutral (green triangles), hydrophobic (red circles). Results are compared with the experimental results in Ref. [47] and with the numerical results in [32]. Our numerical investigation agrees well with the previous numerical and experimental results.

IV. RESULTS AND DISCUSSIONS

After the validation of the results in the absence of thermal fluctuations, we switched-on the thermal noise in the LBM simulations and studied the corresponding fluctuations in the particle’s velocity $U_{\text{conf}}^{(z)}$ in the confined environment. As we have seen in the previous section, the friction acting on the particle is clearly affected by confinement, and it increases with respect to the unconfined case. This increase in friction is quantitatively well reproduced by the simulations (cfr. Fig. 2). Fluctuations are added in the LBM in compliance with the fluctuation-dissipation balance [28, 29]; thus - as a first guess - one could invoke a simplified picture based on a Langevin equation for the particle’s velocity in the direction of volume force [48]

$$m_p \frac{dU_{\text{conf}}^{(z)}(t)}{dt} + \gamma_{\text{conf}} U_{\text{conf}}^{(z)}(t) = F_p + \zeta(t), \quad (11)$$

where $m_p = \pi d^3 \rho_p / 6$ represents the particle’s mass. The scalar term $\xi(t)$ stands for the stochastic noise in compliance with the fluctuation dissipation theorem [48], i.e.

$$\langle \zeta(t) \zeta(t') \rangle = 2\gamma_{\text{conf}} k_B T \delta(t - t').$$

Establishing the correspondence between the mesoscale FLBM dynamics (cfr. Section II) and Eq. (11) is not trivial. Indeed, in order to obtain some “hydrodynamic” interpretation of the FLBM one would need to perform a coarse-graining procedure in the kinetic velocity space and invoke some multi-scale expansion technique (e.g. Chapman-Enskog [9]) to find hydrodynamical equations.

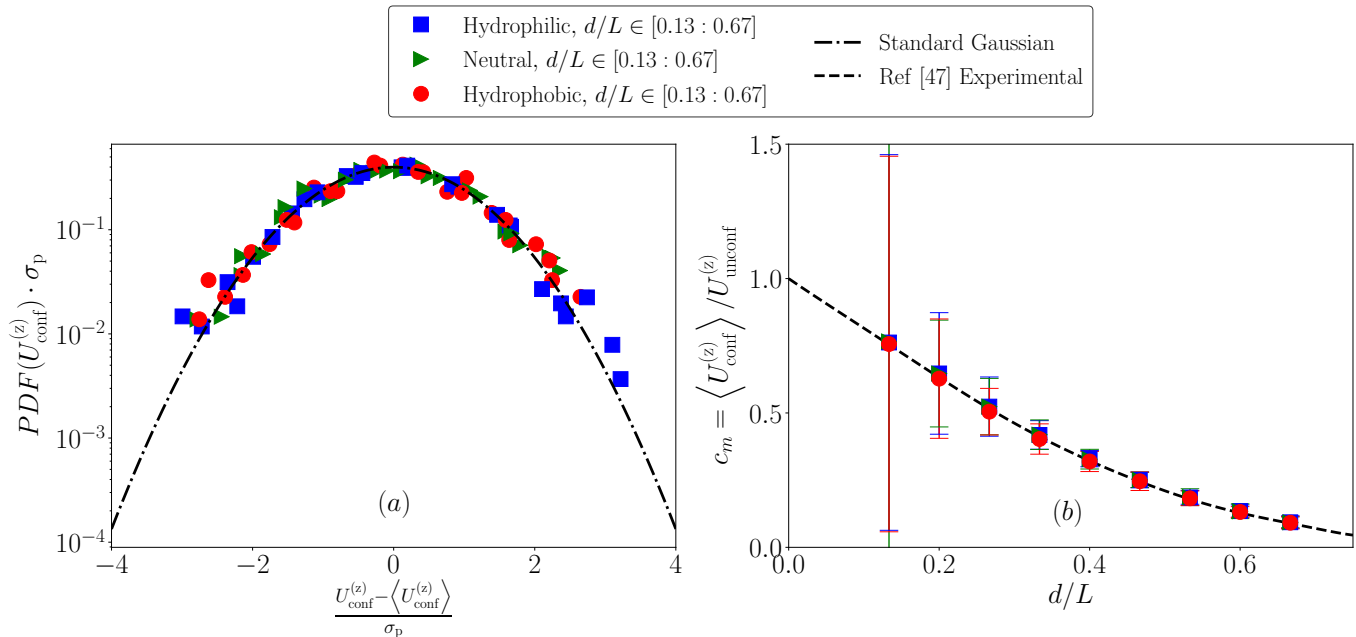


FIG. 3: Panel (a): Standardized PDFs of particle's drift velocity at fixed volume force $g = 5 \cdot 10^{-5}$ (lbu) and fixed thermal energy $k_B T = 0.45 \cdot 10^{-3}$ (lbu). Three different wettabilities were chosen: hydrophilic, neutral and hydrophobic. To make the PDFs comparable with a standard Gaussian distribution, we have considered rescaled variables with zero mean and unitary variance. Data come from different values of the particle diameter $d/L = 0.13, 0.47, 0.67$. Results are matched well with standard Gaussian distribution. Panel (b): we report c_m as function of d/L . The quantity c_m is computed as the ratio between the average particle's drift velocity under confinement and the Stokes' prediction for an unconfined particle driven by the same volume force. Error bars are estimated from standard deviation of the particle's drift velocity fluctuations.

It has to be noted, however, that such a procedure typically requires that fields under study slowly vary in time and space; thus, the “equivalence” between the FLBM simulations and the simple model Eq. (11) could fail. Therefore, it is important to quantitatively investigate if the predictions of Eq. (11) can be matched with the results of the numerical simulations without fitting parameters. Based on this view, we started to analyze the statistical properties in the particle's velocity. The steady state predictions from Eq. (11) imply a Gaussian distribution for the velocity fluctuations

$$P(U_{\text{conf}}^{(z)}) = \sqrt{\frac{1}{2\pi\sigma_p^2}} e^{-\frac{(U_{\text{conf}}^{(z)} - \langle U_{\text{conf}}^{(z)} \rangle)^2}{2\sigma_p^2}} \quad (12)$$

where

$$\langle U_{\text{conf}}^{(z)} \rangle = \frac{F_p}{\gamma_{\text{conf}}} \quad \sigma_p^2 = \frac{k_B T}{m_p}. \quad (13)$$

First of all we checked that $\langle U_{\text{conf}}^{(z)} \rangle = \frac{F_p}{\gamma_{\text{conf}}}$ holds and that the results are compatible with a Gaussian shape. We report in Fig. 3 some representative results for different d/L and different wettabilities, while keeping the volume force and the thermal energy fixed to $g = 5 \cdot 10^{-5}$ lbu and $k_B T = 0.45 \cdot 10^{-3}$ lbu. To check for the Gaussian shape, we report the PDF of the quantity $x = (U_{\text{conf}}^{(z)} - \langle U_{\text{conf}}^{(z)} \rangle)/\sigma_p$. As can be seen, $\langle U_{\text{conf}}^{(z)} \rangle = \frac{F_p}{\gamma_{\text{conf}}}$ holds and the numerical results collapse well on the Gaussian shape $f(x) = e^{-x^2/2}/\sqrt{2\pi}$. We then proceeded in characterizing the dependency of the particle's velocity fluctuations $\Delta U_{\text{conf}}^{(z)} = \sqrt{\sigma_p^2}$ on the three parameters d/L , $k_B T$ and F_p . From Eq. (13) and $m_p = \pi d^3 \rho_p / 6$ one gets

$$\Delta U_{\text{conf}}^{(z)} = \sqrt{\frac{6}{\pi \rho_p L^3}} (k_B T)^{1/2} (d/L)^{-3/2}. \quad (14)$$

The behavior of the velocity fluctuations at changing g , d/L and $k_B T$, is analyzed in Figs. 4 to 6.

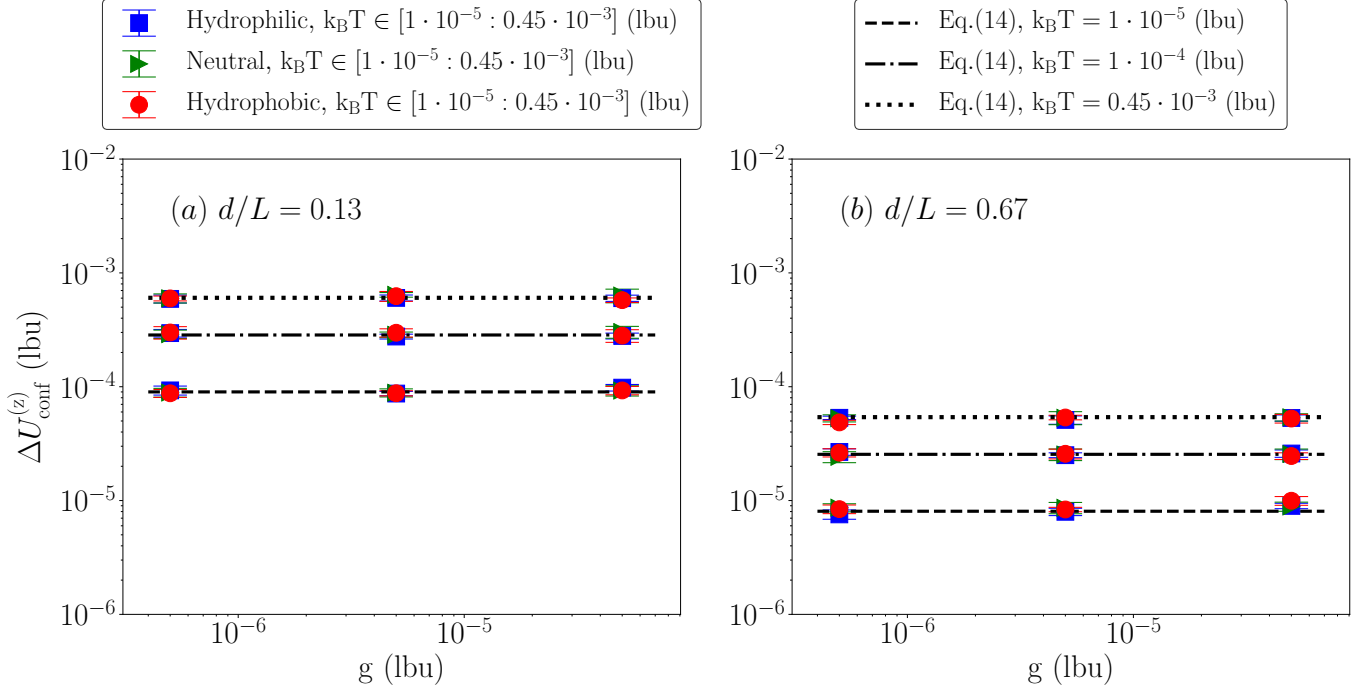


FIG. 4: Particle's velocity fluctuations $\Delta U_{\text{conf}}^{(z)}$ as a function of the volume force g , at changing d/L and thermal energy $k_B T$. Results are compared with the theoretical prediction given in Eq. (14). Panel(a) shows the results under the degree of the confinement $d/L = 0.13$, and Panel (b) presents the results at $d/L = 0.47$. Our simulation data fit well with the theory at all g for Panel(a) and Panel(b). Also, particle's velocity fluctuations show no dependency on the volume force g . When the particle reaches the stationary state, we equally split the data set in five time intervals. Error bars are the standard deviations from different groups of the configurations.

The results are also compared with the prediction of Eq. (14). As predicted by Eq. (14), the velocity fluctuations are independent of the volume force for fixed d/L and $k_B T$ (cfr. Fig. 4); we also observe the scaling $\sim (d/L)^{-3/2}$ for fixed g and $k_B T$ (cfr. Fig. 5) and the scaling $\sim (k_B T)^{1/2}$ for fixed d/L and g (cfr. Fig. 6). To be noticed that not only the scaling laws but also the pre-factor $\sqrt{6/(\pi\rho_p L^3)}$ in Eq. (14) matches very well with the numerical observations. Overall, we observe very little dependency on the particle's wettability.

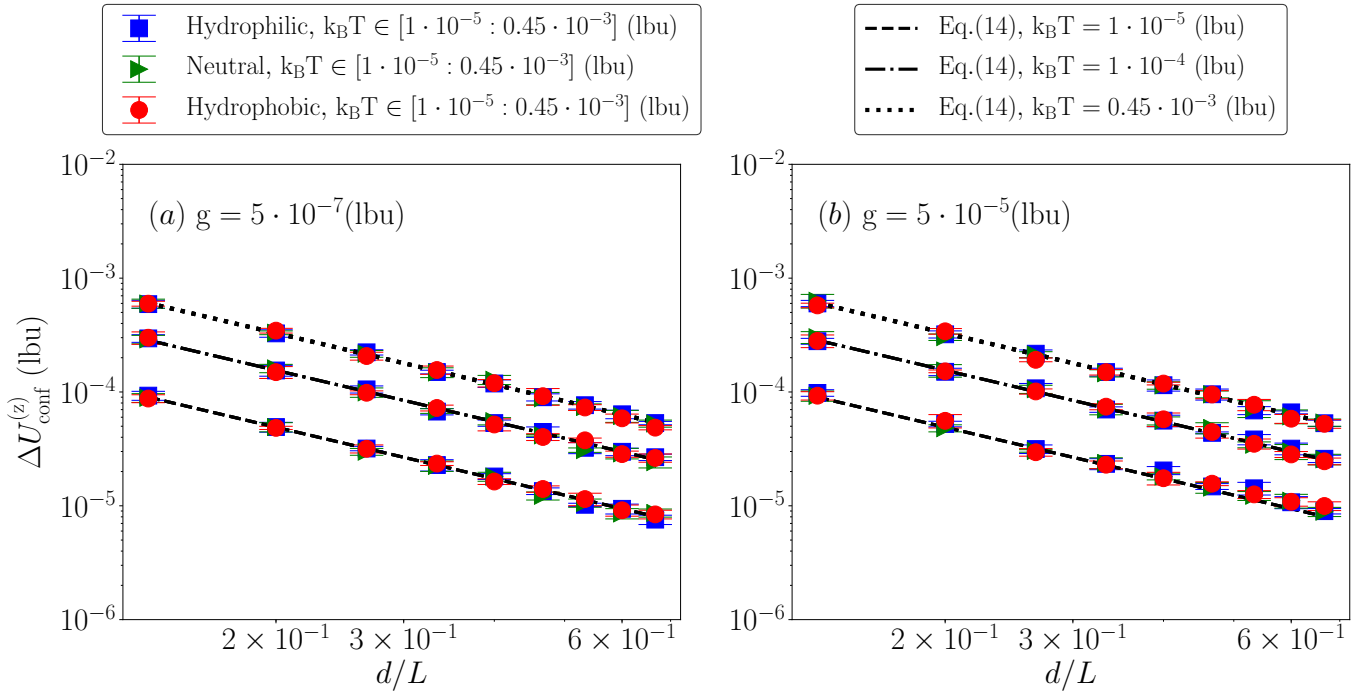


FIG. 5: Particle's velocity fluctuations as a function of d/L at changing the volume force g and the thermal energy $k_B T$. Results are compared with the theoretical prediction given in Eq. (14). Panel(a) shows results at $g = 5 \cdot 10^{-7}$ (lbu), and Panel(b) shows results at largest volume force $g = 5 \cdot 10^{-5}$ (lbu). Three different lines are the theoretical predictions from Eq. (14) at $k_B T = 1 \cdot 10^{-5}, 1 \cdot 10^{-4}, 0.45 \cdot 10^{-3}$ (lbu). Our simulation data fit well with the theory at all d/L . When the particle reaches the stationary state, we equally split the data set in five time intervals. Error bars are the standard deviations from different groups of the configurations.

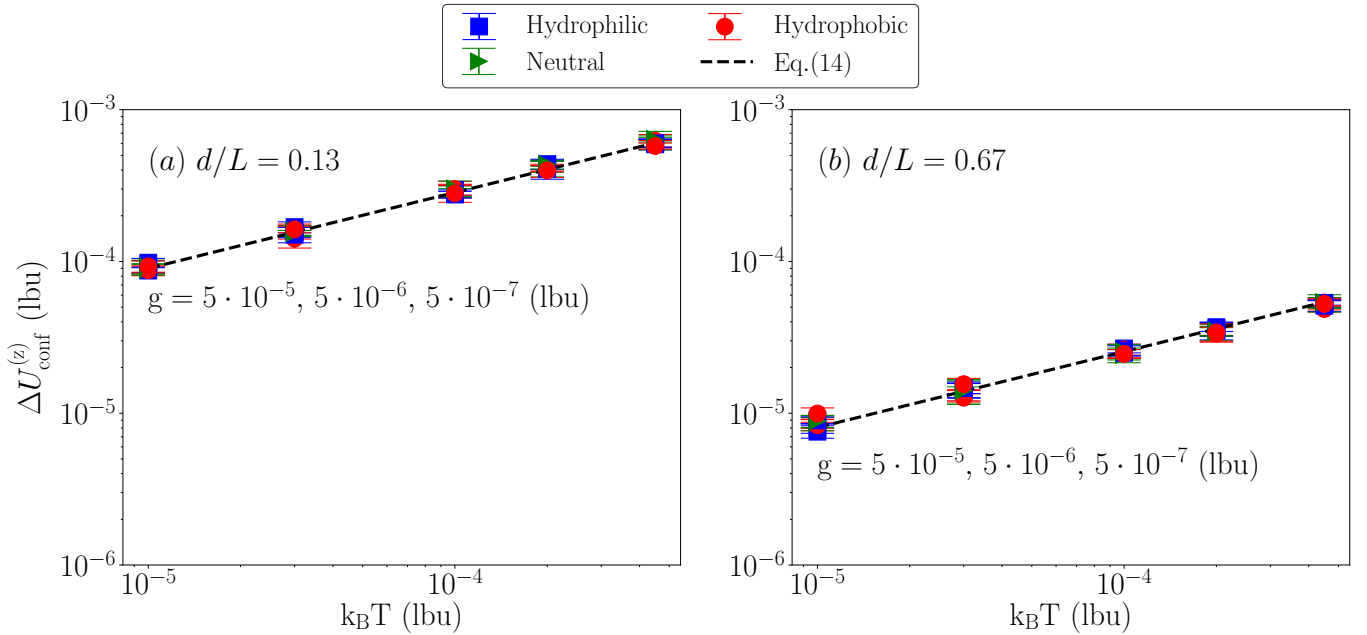


FIG. 6: Particle's velocity fluctuations as a function of the thermal energy $k_B T$ at changing the volume force g and d/L . The back dotted line is the theoretical predictions given in Eq. (14). Panel (a) and (b) shows that simulation data match well with the theory at all $k_B T$ under the volume force $g = 5 \cdot 10^{-5}, 5 \cdot 10^{-6}, 5 \cdot 10^{-7}$ (lbu). When the particle reaches the stationary state, we equally split the data set in five time intervals. Error bars are the standard deviations from different groups of the configurations.

Finally, in Fig. 7 we consider the velocity fluctuations normalized to the mean drift velocity, to highlight the impact of the fluctuations with respect to the characteristic order magnitude of the velocity. Based on Eqs. (10) and (14) and $U_{\text{unconf}}^{(z)} = F_p / \gamma_{\text{unconf}}$, $\gamma_{\text{unconf}} = 3\pi\eta d$, we obtain

$$\frac{\Delta U_{\text{conf}}^{(z)}}{U_{\text{conf}}^{(z)}} = 18 \sqrt{\frac{6\eta^2}{(\rho_A + \rho_B)^2 \pi \rho_p L^7}} \frac{(k_B T)^{1/2} (d/L)^{-7/2} g^{-1}}{c_m} \quad (15)$$

where we have related the particle's velocity to the unconfined velocity via the ratio c_m (cfr. Eq. (10)). To gain insight on the importance of confinement, we also compared the present results with the unconfined predictions $\Delta U_{\text{conf}}^{(z)} / U_{\text{conf}}^{(z)}$ obtained by setting $c_m = 1$ in Eq. (15).

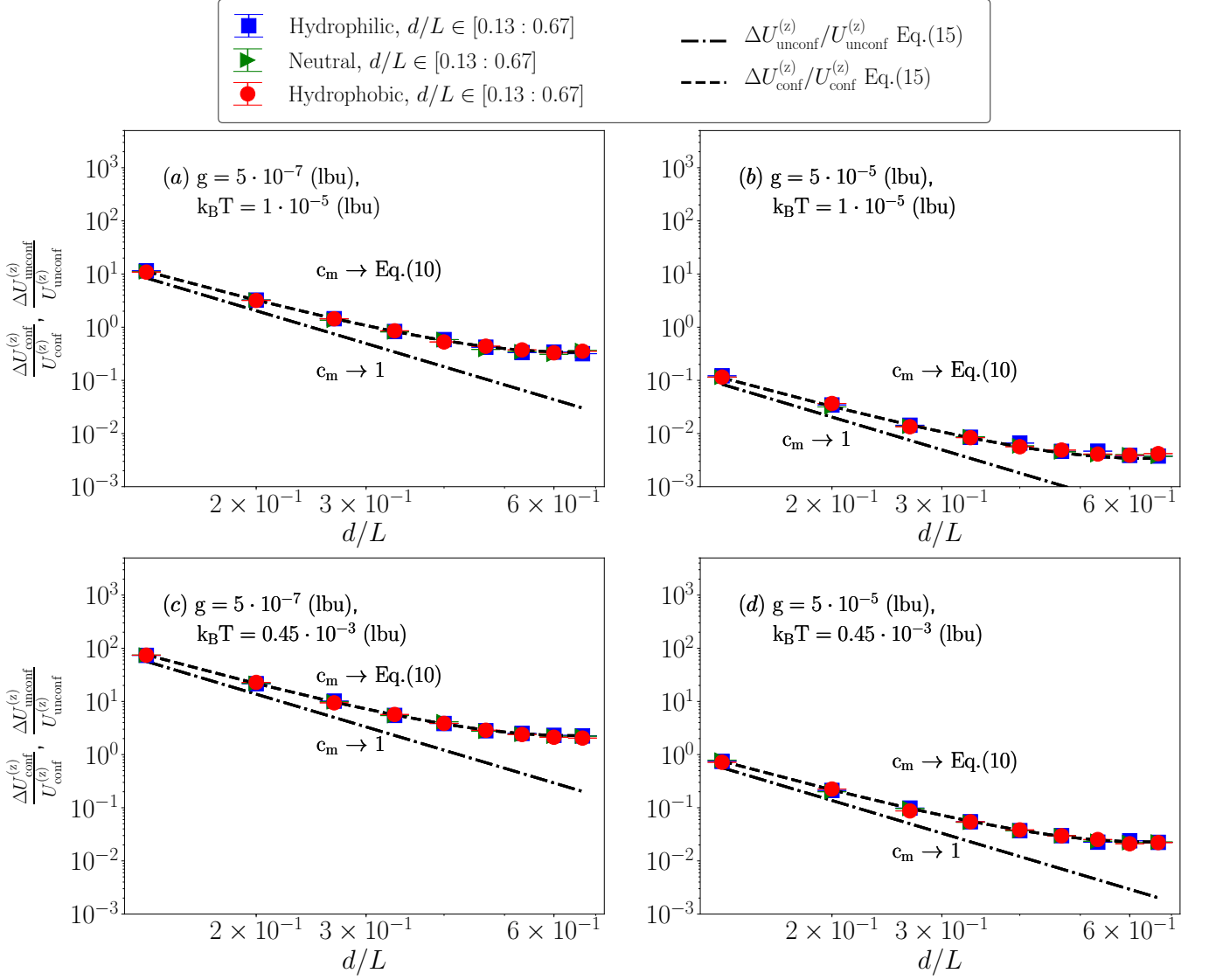


FIG. 7: Particle’s velocity fluctuations normalized to the average velocity in both confined (conf) and unconfined (unconf) environments, as a function of the normalized particle’s diameter d/L . We change both the volume force g and the thermal energy $k_B T$: $g = 5 \cdot 10^{-7}$ lbu, $k_B T = 1 \cdot 10^{-5}$ lbu (Panel (a)), $g = 5 \cdot 10^{-5}$ lbu, $k_B T = 1 \cdot 10^{-5}$ lbu (Panel (b)), $g = 5 \cdot 10^{-7}$ lbu, $k_B T = 0.45 \cdot 10^{-3}$ lbu (Panel (c)), $g = 5 \cdot 10^{-5}$ lbu, $k_B T = 0.45 \cdot 10^{-3}$ lbu (Panel (d)). Theoretical prediction for the confined cases is given in Eq. (15). Theoretical prediction for unconfined cases is obtained using Eq. (15) with $c_m = 1$. Error bars are the standard deviations from different groups of the configurations.

In Fig. 7, we report $\Delta U_{\text{conf}}^{(z)}/U_{\text{conf}}^{(z)}$, $\Delta U_{\text{unconf}}^{(z)}/U_{\text{unconf}}^{(z)}$ at changing d/L for selected values of g and $k_B T$. We also compare with the theoretical predictions obtained from Eq. (15). The numerical data are well in agreement with the theory for all values of d/L . The unconfined theory is well reproduced only at small d/L , as expected. Notice that for the largest d/L we observe a dramatic enhance of the importance of confinement, which is about one magnitude higher than the unconfined theory.

V. CONCLUSIONS

We studied the settling of a spherical particle with diameter d in a fluctuating multicomponent fluid. The system is driven by a constant volume force g in a confined channel with a square cross-sectional area $L \times L$. Our simulations hinge on the fluctuating lattice Boltzmann methodology (FLBM) coupled with a finite-size particle model with tune-

able wettability [33]. We have first validated the numerical set-up in the absence of thermal fluctuations. In agreement with earlier numerical studies [32] on single component LBM, our numerical simulations with the multicomponent LBM well reproduce the frictional properties of a confined particle [47]. We have then switched-on thermal fluctuations, and we have systematically characterized the steady-state statistical properties (i.e. average and fluctuations) of the particle’s velocity at changing the thermal energy $k_B T$, the degree of confinement d/L , the volume force g . The results of the numerical simulations show a neat matching with the predictions of a simplified Langevin-type scenario, accounting for the motion of a particle subject to the linear frictional law induced by confinement and in the presence of a stochastic force satisfying the fluctuation-dissipation theorem [49]. We think this is a nontrivial result since the coarse-grained description of FLBM requires some ”hydrodynamical assumption”, and this could be well violated by the presence of mesoscale fields that do not vary smoothly in space and time. On a quantitative basis, results in the presence of confinement show that the numerical tool is quite versatile in handling quantitative changes in frictional properties across orders of magnitude. Correspondingly, the measured ratio between the velocity fluctuations and the mean velocity comes out to be dramatically increased in the presence of confinement. Having accomplished these steps, the natural follow-up could be represented by the numerical simulations of the particle motion in the presence of a heterogeneous interface [50]. This makes the presented numerical results particularly relevant on the future perspective of achieving a further upgrade of the FLBM simulations as quantitative tools for the study of complex fluids with colloidal particles.

VI. ACKNOWLEDGEMENTS

The authors would like to kindly acknowledge funding from the European Union’s Horizon 2020 research and innovation programme under the Marie Skłodowska-Curie grant agreement No 642069 (European Joint Doctorate Programme “HPC-LEAP”). L. Biferale and M. Sbragaglia acknowledge the support from the ERC Grant No 339032. X.Xue acknowledges fruitful discussions and exchanges with A. Gupta in the early stage of the work.

-
- [1] L.D. Landau, E.M. Lifshitz, *Course of theoretical physics* (Elsevier, 2013)
 - [2] L.E. Reichl. A modern course in statistical physics (1999)
 - [3] F. Toschi, E. Bodenschatz, *Annu. Rev. Fluid Mech.* **41**, 375 (2009)
 - [4] A. Ladd, R. Verberg, *J. Stat. Phys.* **104**(5-6), 1191 (2001)
 - [5] H. Lamb, *Hydrodynamics* (Cambridge university press, 1993)
 - [6] L.M. Milne-Thomson, *Theoretical hydrodynamics* (Courier Corporation, 1996)
 - [7] L.D. Landau, E.M. Lifshitz, *Fluid Mechanics* (Pergamon, 1959)
 - [8] J.M.O. De Zarate, J.V. Sengers, *Hydrodynamic fluctuations in fluids and fluid mixtures* (Elsevier, 2006)
 - [9] S. Succi, *The lattice Boltzmann equation: for fluid dynamics and beyond* (Oxford university press, 2001)
 - [10] J. Wu, C.K. Aidun, *Int. J. Numer. Meth. Fluids.* **62**(7), 765 (2010)
 - [11] N.Q. Nguyen, A.J.C. Ladd, *Phys. Rev. E* **66**(4), 046708 (2002)
 - [12] X. He, S. Chen, R. Zhang, *J. Comput. Phys.* **152**(2), 642 (1999)
 - [13] H. Liu, A.J. Valocchi, Q. Kang, *Phys. Rev. E* **85**(4), 046309 (2012)
 - [14] T. Reis, T. Phillips, *J. Phys. A* **40**(14), 4033 (2007)
 - [15] D. Chiappini, M. Sbragaglia, X. Xue, G. Falcucci, *Phys. Rev. E* **99**, 053305 (2019)
 - [16] D. Chiappini, X. Xue, G. Falcucci, M. Sbragaglia, *AIP Conf. Proc.* **1978**(1), 420003 (2018)
 - [17] F. Milan, M. Sbragaglia, L. Biferale, F. Toschi, *Eur. Phys. J. E* **41**(1), 6 (2018)
 - [18] P. Ahlrichs, B. Dünweg, *J. Chem. Phys.* **111**(17), 8225 (1999)
 - [19] P. Ahlrichs, B. Dünweg, *Int. J. Mod. Phys. C* **9**(08), 1429 (1998)
 - [20] O. Berk Usta, A.J. Ladd, J.E. Butler, *J. Chem. Phys.* **122**(9), 094902 (2005)
 - [21] J. de Graaf, H. Menke, A.J. Mathijssen, M. Fabritius, C. Holm, T.N. Shendruk, *J. Chem. Phys.* **144**(13), 134106 (2016)
 - [22] M. Gross, M.E. Cates, F. Varnik, R. Adhikari, *J. Stat. Mech.: Theory and Exp.* **3**, P03030 (2011)
 - [23] A. Ladd, *J. Fluid Mech.* **271**, 285 (1994)
 - [24] R. Adhikari, K. Stratford, M.E. Cates, A.J. Wagner, *Europhys. Lett.* **71**, 473 (2005)
 - [25] B. Dünweg, U.D. Schiller, A.J.C. Ladd, *Phys. Rev. E* **76**, 036704 (2007)
 - [26] M. Gross, R. Adhikari, M.E. Cates, F. Varnik, *Phys. Rev. E* **82**, 056714 (2010)
 - [27] G. Kaehler, A.J. Wagner, *Phys. Rev. E* **87**, 063310 (2013)
 - [28] D. Belardinelli, M. Sbragaglia, L. Biferale, M. Gross, F. Varnik, *Phys. Rev. E* **91**, 023313 (2015)
 - [29] D. Belardinelli, M. Sbragaglia, R. Benzi, S. Ciliberto, *Phys. Rev. E* **99**, 063302 (2019)
 - [30] X. Xue, M. Sbragaglia, L. Biferale, F. Toschi, *Phys. Rev. E* **98**(1), 012802 (2018)
 - [31] A.J. Ladd, *J. Fluid Mech.* **271**, 285 (1994)
 - [32] C.K. Aidun, Y. Lu, E.J. Ding, *J. Fluid Mech.* **373**, 287 (1998)

- [33] F. Jansen, J. Harting, Phys. Rev. E **83**(4), 046707 (2011)
- [34] T. Krüger, H. Kusumaatmaja, A. Kuzmin, O. Shardt, G. Silva, E.M. Viggien, Springer International Publishing **10**, 978 (2017)
- [35] D. d’Humières, I. Ginzburg, M. Krafczyk, P. Lallemand, L.S. Luo, Phil. Trans. Roy. Soc. London, Ser. A **360**, 437 (2002)
- [36] U.D. Schiller, Thermal fluctuations and boundary conditions in the lattice boltzmann method. Ph.D. thesis, Johannes Gutenberg-Universität, Mainz (2008)
- [37] X. Shan, H. Chen, Phys. Rev. E **47**, 1815 (1993)
- [38] X. Shan, H. Chen, Phys. Rev. E **49**, 2941 (1994)
- [39] J. Zhang, Microfluid. Nanofluid. **10**, 1 (2011)
- [40] M. Sbragaglia, D. Belardinelli, Phys. Rev. E **88**, 013306 (2013)
- [41] M. Sega, M. Sbragaglia, S.S. Kantorovich, A.O. Ivanovd, Soft Matter **9**, 10092 (2013)
- [42] M.P. Allen, D.J. Tildesley, *Computer simulation of liquids* (Oxford university press, 2017)
- [43] J. Happel, H. Brenner, *Low Reynolds number hydrodynamics: with special applications to particulate media*, vol. 1 (Springer Science & Business Media, 2012)
- [44] P. Ganatos, R. Pfeffer, S. Weinbaum, J. Fluid Mech. **99**(4), 755 (1980)
- [45] P. Ganatos, S. Weinbaum, R. Pfeffer, J. Fluid Mech. **99**(4), 739 (1980)
- [46] H.J. Keh, P.Y. Chen, Chem. Eng. Sci. **56**(24), 6863 (2001)
- [47] A. Miyamura, S. Iwasaki, T. Ishii, Int. J. Multiphase Flow **7**(1), 41 (1981)
- [48] H. Risken, in *The Fokker-Planck Equation* (Springer, 1996), pp. 63–95
- [49] R. Kubo, Rep. Prog. Phys. **29**(1), 255 (1966)
- [50] G. Boniello, C. Blanc, D. Fedorenko, M. Medfai, N.B. Mbarek, M. In, M. Gross, A. Stocco, M. Nobili, Nat. Mater. **14**(9), 908 (2015)